185. A Tricyclic Template Derived from (2*S*,4*R*)-4-Hydroxyproline for the Synthesis of Protein Loop Mimetics

by **Reto Beeli, Mathias Steger, Anthony Linden**, and **John A. Robinson***

Institute of Organic Chemistry, University of Zurich, Winterthurerstrasse 190, CH–8057 Zurich

(30.VIII.96)

A tricyclic diketopiperazine, formally derived by coupling (2*S*,4*S*)-4-aminoproline (Pro(NH_2)) and (2*S*,4*R*)-4-(carboxymethyl)proline (Pro(CH_2COOH)), is synthesized starting from readily available (2*S*,4*R*)-4-hydroxyproline. The resulting tricyclic template has carboxy and amino groups to which a peptide chain may be attached. The Fmoc-protected template **5** is incorporated into the cyclic molecule cyclo(-Ala^1-Asn^2-Pro^3-Asn^4-Ala^5-Ala^6-⌐ $Pro(NH_2)^7$ = $Pro(CH_2COOH)^8$ ⌐-) (**6**) where $Pro(NH_2)^7$ = $Pro(CH_2COOH)^8$ represents the template, using solid-phase peptide synthesis with cyclization in solution. The molecule is shown by NMR and dynamic simulated annealing methods to adopt a preferred conformation in aqueous solution, which includes an extended backbone at the residues Asn^2-Pro^3-Asn^4, and a type-I β-turn at Asn^4-Ala^5-Ala^6-⌐ $Pro(NH_2)^7$. These studies show that this novel template may be used in the synthesis of cyclic peptide and protein mimetics having defined secondary structure in aqueous environments.

Introduction. – Relative rigid organic molecules containing functional groups to which a peptide chain may be attached are of potential interest as templates in the design of novel peptide and protein mimetics. The conformational and biological properties of surface loops on proteins, *e.g.*, may be mimicked in some cases by small synthetic molecules in which the peptide sequence is grafted from the protein of interest onto a suitable template molecule [1–4]. However, the conformations induced in the template-bound peptide loop will clearly be dependent on the geometry of the template and the relative location and orientation of the anchoring groups. We have reported previously [5] [6] the bicyclic templates **1** and **2** and demonstrated their use in the synthesis of loop mimetics **3** and **4** containing the hexapeptide Ala-Asn-Pro-Asn-Ala-Ala (ANPNAA) (*Scheme 1*). Within this sequence is an NPNA motif which is found as a tandemly repeated unit in the circumsporozoite surface protein of the malaria parasite *Plasmodium falciparum*. Linear synthetic peptides containing repeated NPNA motifs have a weak tendency to adopt type-I β-turn conformations based on the NPNA cadence [7] [8], whereas both **3** and **4** were shown to adopt a stabilized type-I β-turn conformation in the NPNA motif in aqueous solution [5] [6].

(2*S*,4*R*)-4-Hydroxyproline is an attractive building block for template design because it is a relatively rigid amino acid that can be readily functionalized. Here we describe the synthesis of a new tricyclic template **5** and its incorporation into the loop mimetic **6**, which again contains the hexapeptide sequence ANPNAA (*Scheme 2*). This also provides an opportunity to compare the template-induced conformation of the NPNA motif in **6** with that observed in **3** and **4**. The conformational behaviour of **6** in aqueous solution was investigated using NMR and dynamic restrained simulated annealing methods.

Scheme 1

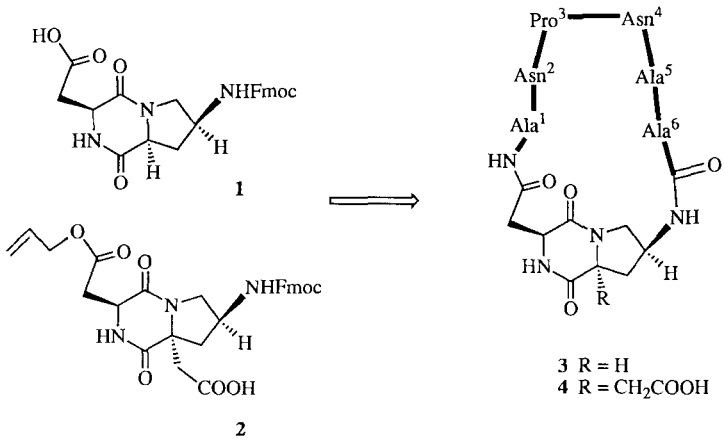

Scheme 2

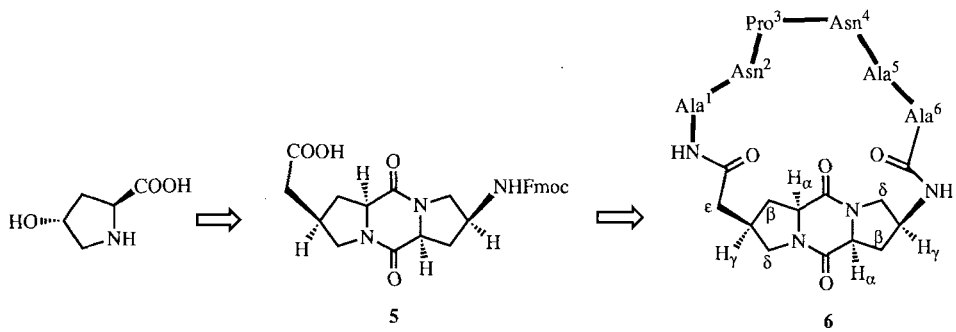

Results and Discussion. – *Synthesis.* Template **5** was synthesized from (2*S*,4*R*)-4-hydroxyproline following the route shown in *Scheme 3*. A *Mitsunobu* reaction [9] was used to indroduce the N-substituent at C(4) in **7**, as reported in earlier work [6]. The coupling of **7** and *N*-(benzyloxycarbonyl)-4-hydroxyproline (**8**) was effected with HBTU[1]) for activation. Upon removal of the Z-protecting group (Z = benzyloxycarbonyl) in the resulting dipeptide, cyclization proceeded *in situ* to afford **9**. The carboxymethyl side chain was then appended to **9** by oxidation of the alcohol function, followed by a *Wittig* reaction and hydrogenation. This last step afforded the *cis*-isomer with high diastereoselectivity (> 95% de). Exchange of the phthalimide group (Phth) for a Fmoc-protecting group (Fmoc = (9*H*-fluoren-9-ylmethoxy)carbonyl) afforded **5**, whose structure was confirmed by X-ray crystallography.

[1]) See *Exper. Part* for abbreviations of reagents.

Scheme 3[1])

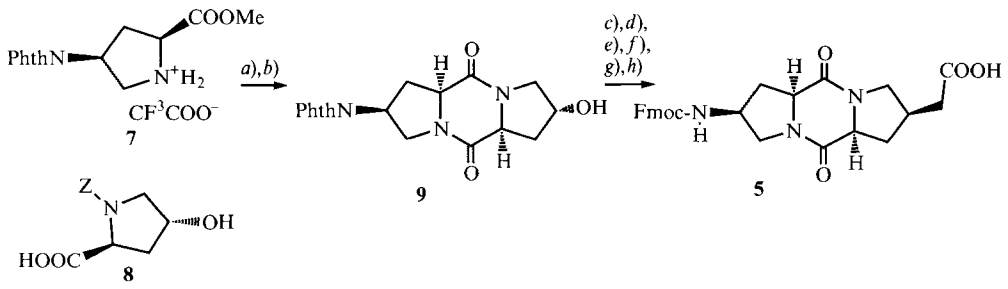

a) (i-Pr)$_2$EtN, HBTU (65%). *b*) H_2, Pd/C (72%). *c*) Py·SO_3 (89%). *d*) $(MeO)_2P(O)CH_2COOMe$, $(Me_3Si)_2NNa$ (96%). *e*) H_2, Pd (60%). *f*) NH_2NH_2, EtOH. *g*) LiOH. *h*) Fmoc-Cl (55%).

Crystals of **5** were obtained from MeOH as very thin plates, which were weakly diffracting and gave rather poor refinement results. The resulting geometric parameters are, therefore, of limited accuracy although the conformation is clearly defined. The asymmetric unit in the unit cell contained two molecules of **5**, which differ mainly in the torsion angles linking the Fmoc group to the tricyclic template and in the orientation of the carboxylic-acid group. The molecules are linked in the crystal by H-bonds into infinite one-dimensional chains, each chain containing only one type of independent molecule (*i.e.* either ...AAA... or ...BBB...). The A and B chains are cross-linked to each other by additional H-bonds to form columns of molecules which run parallel to the *z*-axis. ORTEP Diagrams of these two crystal conformations are shown in *Fig. 1*. The torsion angles within the pyrrolidine rings of each crystal conformation are given for both molecules in *Table 1*. The two conformers could be superimposed in the atoms constituting the tricyclic diketopiperazine (C(α), C′, N, C(β), C(γ), C(δ)) with an r.m.s. deviation of 0.22 Å.

The cyclic template-bound loop mimetic **6** was then prepared by the route shown in *Scheme 4*. The linear sequence **10** was first constructed by solid-phase synthesis using Fmoc chemistry [10] on the acid-sensitive resin *Tentagel-SAC* (*Rapp Polymere*, Tübingen). After assembly, **10** was cleaved from the solid-support using 1% CF_3COOH/CH_2Cl_2, without removal of the side chain protecting groups. Cyclization was then performed in dilute solution (*ca.* 0.8 μM), using HATU and HOAt for activation [11][1]), the side chain protecting groups were removed, and the product was purified by reversed-phase HPLC.

Conformational Studies by NMR. The conformation of **6** was investigated by ^{1}H-NMR spectroscopy in aqueous solution (H_2O/D_2O 9:1, pH 5). The 1D spectrum of **6** reveals only a single species (> 98%) on the NMR time scale. The spectrum was assigned by standard methods [12] using COSY, TOCSY, and ROESY (*Table 2*). Stereospecific assignments were possible for the four methylene groups in the pyrrolidine rings of the template, as well as for the side chain 2 H–N(δ) protons of Asn^2 and Asn^4. However, stereospecific assignments for the 2 H–C(β) protons in Asn^2 and Asn^4, the methylene groups in Pro^3, and the 2 H–C(ε) group in the Pro$(CH_2COOH)^8$ moiety in the template, were not obtained unambiguously. The chemical shift of the Pro$(NH_2)^7$NH–C(γ) (7.46 ppm) lies upfield of the values observed for the corresponding protons in the major

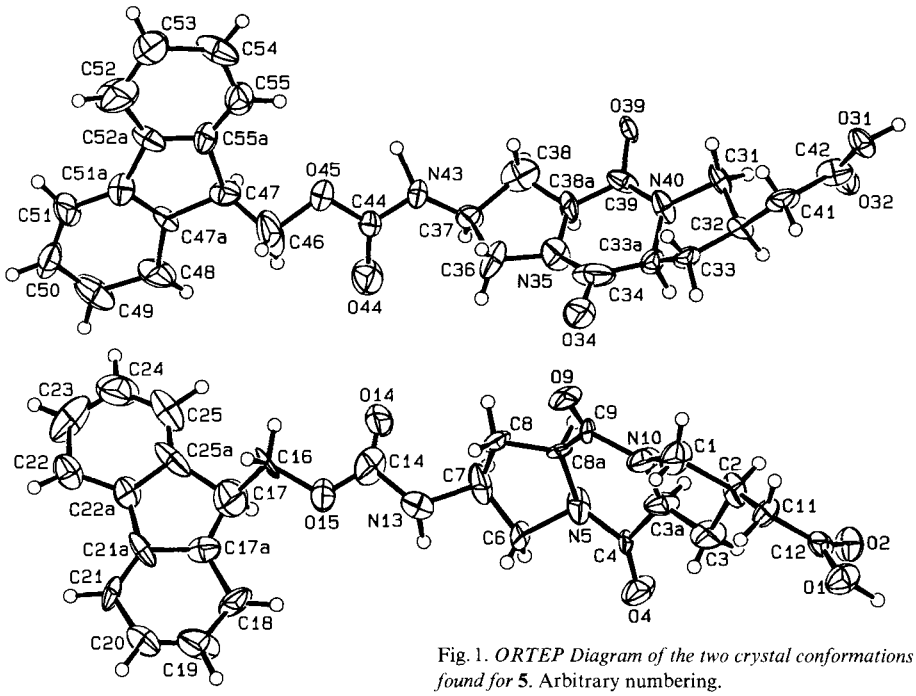

Fig. 1. *ORTEP Diagram of the two crystal conformations found for* **5**. Arbitrary numbering.

Table 1. *Side-Chain Torsion Angles in the Two Conformations Seen in the Crystal Structure of* **5** (see *Fig. 1*). Note $\chi_5 = C(\gamma)-N-C(\alpha)-C(\beta)$ torsion; $\chi_{3'} = C(\beta)-C(\gamma)-N-C'$ in Pro(NH_2)[7] and $\chi_{3'} = C(\beta)-C(\gamma)-C(\varepsilon)-C'$ in Pro(CH_2COOH)[8]. Standard deviations are in brackets.

Conformer A			Conformer B		
Torsion	Pro(NH_2)[7]	Pro(CH_2COOH)[8]	Torsion	Pro(NH_2)[7]	Pro(CH_2COOH)[8]
χ_1	−12 (1)	−25 (2)	χ_1	−18 (2)	−34 (1)
χ_2	31 (1)	40 (1)	χ_2	28 (1)	38 (1)
χ_3	−37 (1)	−39 (1)	χ_3	−28 (1)	−25 (1)
χ_4	29 (1)	27 (1)	χ_4	21 (2)	6 (1)
χ_5	−10 (1)	−3 (2)	χ_5	−2 (2)	17 (1)
$\chi_{3'}$	61 (2)	69 (1)	$\chi_{3'}$	162 (1)	−180 (1)

Scheme 4[1])

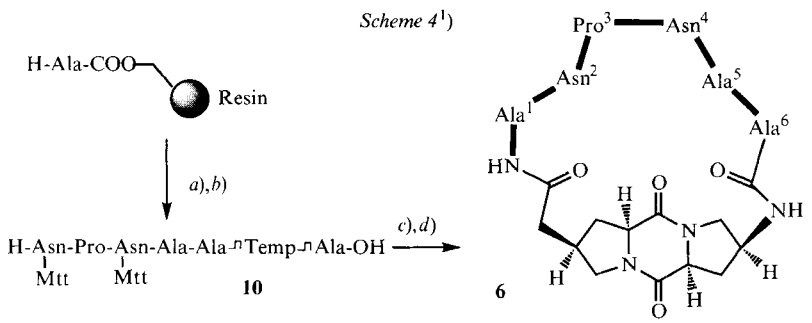

a) For each coupling: Fmoc-Xaa-OH or **5** (4 equiv.), HBTU, HOBt, $(i\text{-}Pr)_2EtN$, DMF, then 20% piperidine in DMF. *b*) 1% CF_3COOH in CH_2Cl_2 (38%). *c*) HATU, HOAt, $(i\text{-}Pr)_2EtN$, DMF. *d*) $CF_3COOH/H_2O/Me_3SiH$ 95:2.5:2.5 (40%).

conformers deduced for mimetics **3** and **4** (8.25 and 8.46 ppm, resp. [5] [6]), and is outside the range (8.3–8.7 ppm) normally seen for peptide NHs in random-coil peptides under these conditions [13]. This is noteworthy, since other NMR data (*vide infra*) strongly implicate this NH in intramolecular H-bonding. There are no significant changes in chemical shifts for **6** in the concentration range 1–15 mM, nor as the pH is varied from 3.0 to 7.0 (in H_2O/D_2O 9:1 at 300 K).

Table 2. *^{1}H-NMR* (600 MHz) *Chemical Shifts for* **6** *at 300 K in 10% $^2H_2O/H_2O$ at pH 5.0*

	Chemical shift [ppm][a])			
Residue[b])	NH	H–C(α)	$CH_2(\beta)$ or Me(β)[c])	Others[c])
Ala[1]	8.43	4.125	1.38	
Asn[2]	7.98	4.88	2.52, 2.78	7.64 (NH, *trans*[d])), 6.94 (NH, *cis*[d]))
Pro[3]		4.61	1.89, 2.16	1.98, 2.08 ($CH_2(\gamma)$); 3.63, 3.85 ($CH_2(\delta)$)
Asn[4]	8.04	4.82	2.84, 3.07	7.52 (NH *trans*[d])); 6.70 (NH, *trans*[d]))
Ala[5]	8.30	4.120	1.41	
Ala[6]	7.90	4.121	1.35	
Pro(NH_2)[7]	7.46	4.56	*2.29, 2.64*	4.45 (H–C(γ)); *3.68, 3.98* ($CH_2(\delta)$)
Pro(CH_2COOH)[8]		4.51	1.83, 2.38	2.67 (H–C(γ)); *3.74, 3.08* ($CH_2(\delta)$); 2.42, 2.76 ($CH_2(\varepsilon)$)

[a]) Chemical shifts are measured relative to internal TSP (= sodium 3-(trimethylsilyl)(D_4)propanoate). Pro(NH_2)[7] and Pro(CH_2COOH)[8] are the 4-aminoproline and 4-(carboxymethyl)proline moieties of the template, respectively.

[b]) The Pro(NH_2)[7]NH refers to NH–C(γ), and the Pro(CH_2COOH)[8] $CH_2(\varepsilon)$ refers to the CH_2 of the 4-(carboxymethyl) substituent on the proline ring.

[c]) Stereospecific assignments are in *italics*, in the order *pro-R, pro-S*.

[d]) *cis* and *trans* with respect to =O of the $CONH_2$ group.

Observed Coupling Constants. ^3J(H,H) coupling constants for **6** measured from 1D spectra and by E.COSY are given in *Table 3*. The values observed give useful information about the range of conformations populated by **6** in aqueous solution. Firstly, the observed ^3J values within the Pro(NH_2)[7] moiety in the template lie mostly in the range 5–8 Hz, which is indicative of conformational averaging through rapid ring flipping between folded (envelope) and twist conformations. However, within the Pro(CH_2COOH)[8] moiety of the template, the ^3J values > 11 Hz reveal a stable ring pucker, similar to that seen in the crystal structure of **5** (*Fig. 1*). The $^3J(\alpha,\beta)$, $^3J(\beta,\gamma)$, and $^3J(\gamma,\delta)$ values observed in the pyrrolidine ring of Pro(CH_2COOH)[8] in **6**, are close to those predicted by the *Karplus* relationship [14], based on the dihedral angles found for this ring in the crystal structures of **5** (*Table 1*). The combination of large and small $^3J(\gamma,\varepsilon)$ and $^3J(\gamma,\varepsilon')$ values also indicate a preferred conformation for the carboxymethyl side chain in Pro(CH_2COOH)[8], although the lack of a stereospecific assignment for the methylene group precludes a definition of the preferred torsion angle. The $^3J(\alpha,\beta)$ values for the two Asn residues also indicate preferred, albeit different side-chain conformations. Finally, the Ala[1] and Ala[5] $^3J(\alpha$,NH) values lie outside the range (6.5–8.0 Hz) normally associated with fast conformational averaging, indicating that the peptide backbone around these residues adopts a preferred conformation.

Table 3. *Coupling Constants* J[a]) [Hz] *for* **6**

Residue	$^3J(\alpha,NH)$	$^3J(\alpha,\beta)$	Others
Ala[1]	4.8	7.2	
Asn[2]	8.1	5.0, 9.0[b])	$J(\beta,\beta')$ = 14.5
Pro[3]	–	7.1, 7.5[b])	n.d.
Asn[4]	8.4	4.7, 5.2[b])	$J(\beta,\beta')$ = 16.5
Ala[5]	3.6	7.3	
Ala[6]	5.7	7.2	
Pro(NH_2)[7]	(6.6[c]))	8.6, 7.8[d])	$J(\beta_{pro\text{-}R},\gamma)$ = 6.2, $J(\beta_{pro\text{-}S},\gamma)$ = 6.4, $J(\beta,\beta')$ = 13.3, $J(\gamma,\delta_{pro\text{-}R})$ = 7.3, $J(\gamma,\delta_{pro\text{-}S})$ = 4.4, $J(\delta,\delta')$ = 12.7, $J(\alpha,\alpha')$ = 2.2[e])
Pro(CH_2COOH)[8]		11.5, 6.0[d])	$J(\beta_{pro\text{-}R},\gamma)$ = 11.5, $J(\beta_{pro\text{-}S},\gamma)$ = 5.8, $J(\beta,\beta')$ = 11.8, $J(\gamma,\delta_{pro\text{-}R})$ = 8.3, $J(\gamma,\delta_{pro\text{-}S})$ = 11.8, $J(\delta,\delta')$ = 11.5, $J(\delta,\varepsilon)$ = 9.4[b]), $J(\delta,\varepsilon')$ = 3.3[b]), $J(\varepsilon,\varepsilon')$ = 16.6

[a]) Measured from 1D spectra and/or by E.COSY. [b]) Stereospecific assignments not available. [c]) Refers to the ^3J(NH–C(γ),H–C(γ)) coupling. [d]) Given in the order *pro-R*, *pro-S*. [e]) $J(\alpha,\alpha')$ = ^5J(H,H) of Pro(NH_2)[7]H–C(α) to Pro(CH_2COOH)[8] H–C(α).

H/D Exchange and Temperature Coefficients. H/D Exchange rates of amide NH groups and the temperature dependencies of their chemical shifts provide complementary information which may be used to identify likely intramolecular H-bond donors. The temperature coefficients for the amide NH protons are given in *Table 4*. The range –7 to –9 ppb/K is normally associated with exposed peptide NH groups in random-coil peptides [13], whereas smaller values may indicate shielding from the solvent and possible involvement in intramolecular H-bonding. On this basis, the coefficient close to zero for the Pro(NH_2)[7]NH is noteworthy, as are the small values for Ala[6]NH and Asn[2]NH, and for the H_{cis}–N(δ) in the side chain of Asn[4]. H/D Exchange rates were measured in 100% D_2O at pD* 3.5, by monitoring residual NH signal intensities *vs.* time. Most of the NH signals for **6** had disappeared from the 1D ^{1}H-NMR spectrum within a few minutes, except those for Pro(NH_2)[7], Asn[4], and Ala[6]. The half-life for Pro(NH_2)[7]NH was *ca.* 1 h, whereas the H/D exchange for Asn[4]NH and Ala[6]NH was complete in *ca.* 1.5 h and 30 min, respectively. The slow exchange rate of the Pro(NH_2)[7]NH correlates with its temperature coefficient close to zero, and both point to the involvement of this group in intramolecular H-bonding. The correlation is poor, however, with Asn[4]NH, whose temperature coefficient is large, although is exchange rate is relatively slow (*vide infra*).

Table 4. *Amide NH* ^{1}*H-NMR Chemical Shift Temperature Coefficients* $\Delta\delta$/K [ppb/K] *for* **6**

	Ala[1]	Asn[2]	Asn[4]	Ala[5]	Ala[6]	Pro(NH_2)[7]	Asn[2]H–N(δ)[a])		Asn[4]H–N(δ)[a])	
							trans	*cis*	*trans*	*cis*
Temp. coeff.[b])	–10.4	–3.3	–7.2	–5.7	–2.6	0.0	–7.8	–5.9	–4.0	–2.5

[a]) *cis* and *trans* with respect to =O of the $CONH_2$ group.

[b]) The coefficients for backbone and side-chain amide NHs are given. Pro(NH_2)[7] is the 4-aminoproline moiety in the template. Measurements were made in aq. solution (H_2O/D_2O 9:1), pH 5.0, over the temperature range 278–315 K.

NOE Connectivities. Peptide **6** is small and most likely retains significant conformational mobility, so averaging of the signals obtained from NOESY and *J*-coupling would be expected. Nevertheless, the NOE averaging is dominated by short distances due to the r^{-6} distance dependence, and fast motions (*ca.* 10^{-9} s) can reduce the number of observed NOEs. Therefore, the appearance of a network of long-range NOE connectivities (*i.e.* not intra-residue or sequential (i, $i+1$) NOEs) in **6** (*Table 5*) already provides an indication that compact folded conformations are significantly populated on the NMR time scale. NOE Connectivities in **6** were identified by ROESY with mixing times (spin-lock periods) of 75, 150, 225, 300, and 375 ms. NOEs are observed between protons in the template and Pro^3/Asn^4, showing that conformations are present in solution with Pro^3 and Asn^4 packed close to the template. NOEs indicative of a β-turn within the NPNA motif (as seen earlier in **3** and **4** [5] [6]) were not observed. However, a relatively strong $d(NH^i, NH^{i-1})$ NOE connectivity between Ala^6 and Pro(NH$_2$)^7 is present, consistent with a β-turn at Asn^4-Ala^5-Ala^6 ⌐ Pro(NH$_2$)^7. The temperature coefficients (*Table 4*) and H/D exchange data also implicate the Pro(NH$_2$)^{7}NH in intramolecular H-bonding, as would be expected in a H-bond-stabilized β-turn.

Table 5. *The Strong, Medium, and Weak ^{1}H,^{1}H-NOE Connectivities*[a]) *Used for the Derivation of Distance Restraints in Simulated Annealing Calculations*

Strong NOEs (up to 2.5 Å)		Weak NOEs (up to 5.0Å)	
Pro^{7}NH	Pro^{7}H$_{pro\text{-}S}$–C(δ)	Asn^{4}NH	Pro^{7}H$_{pro\text{-}S}$–C(δ)
		Asn^{4}NH	Pro^{7}H$_{pro\text{-}R}$–C(β)
		Asn^{4}NH	Pro^{8}H$_{pro\text{-}R}$–C(β)
Medium NOEs (up to 3.0Å)		Asn^{4}H$_{cis}$–N(δ)	Pro^{8}H–C(ε)
Ala^{6}NH	Pro^{7}NH	Asn^{4}H$_{cis}$–N(δ)	Ala^{6}H–C(β)
Asn^{2}NH	Ala^{1}H–C(α)	Asn^{4}H$_{trans}$–N(δ)	Ala^{6}H–C(β)
Ala^{6}NH	Ala^{6}H–C(α)	Ala^{6}NH	Asn^{4}H′–C(β)
Pro^{7}NH	Pro^{7}H$_{pro\text{-}R}$–C(β)	Ala^{6}NH	Asn^{4}H–C(β)
Asn^{2}H$_{trans}$–N(δ)	Asn^{2}H–C(β)	Asn^{2}H$_{cis}$–N(δ)	Ala^{1}H–C(β)
Asn^{4}H$_{trans}$–N(δ)	Asn^{4}H–C(β)	Asn^{2}H$_{trans}$–N(δ)	Ala^{1}H–C(β)
Ala^{1}NH	Pro^{8}H–C(ε)	Pro^{3}H–C(β)	Pro^{7}H$_{pro\text{-}S}$–C(δ)
Asn^{4}NH	Pro^{3}H–C(α)	Pro^{8}H$_{pro\text{-}S}$–C(β)	Pro^{3}H–C(α)
Asn^{2}H′–C(β)	Pro^{3}H–C(δ)	Pro^{8}H$_{pro\text{-}R}$–C(β)	Pro^{3}H–C(α)
Pro^{8}H–C(ε)	Pro^{8}H$_{pro\text{-}S}$–C(δ)	Pro^{7}H$_{pro\text{-}R}$–C(β)	Ala^{6}H–C(β)
Pro^{7}H–C(α)	Pro^{7}H$_{pro\text{-}S}$–C(β)	Pro^{8}H′–C(ε)	Ala^{1}H–C(α)
Pro^{8}H$_{pro\text{-}R}$–C(β)	Pro^{8}H$_{pro\text{-}S}$–C(δ)	Asn^{2}NH	Pro^{8}H–C(ε)

[a]) Pro^7 refers to Pro(NH$_2$)^7, and Pro^8 refers to Pro(CH$_2$COOH)^8.

Structure Calculations. To determine possible folded conformations for **6**, average solution structures were calculated by restrained dynamic simulated annealing (SA) [15], using the observed NOE connectivities in *Table 5* to derive distance restraints as input with the CVFF force field in the DISCOVER program (*Biosym*, San Diego). These calculations yielded 31 out of 50 structures that have no NOE violations ≥ 0.27 Å, and all of which are within 10 kcal/mol of the lowest-energy conformer (*Table 6*). A superimposition reveals convergence to a family of closely related conformations, with a pairwise r.m.s. deviation of 0.4 ± 0.17 Å (range 0.002–0.91 Å) over the atoms C(α), C′, and N of

the backbone (*Fig. 2*). A typical low-energy structure is shown in *Fig. 3* (see *Table 7* for torsion angles). In this conformation, the residues Asn[4], Ala[5], Ala[6], and Pro(NH$_2$)[7] adopt a type-I β-turn, with the Pro(NH$_2$)[7]NH in a position to H-bond with one or both the Asn[4]

Table 6. *Summary of Input Constraints for the Structure Calculations and the Violations, r.m.s. Deviations, and Energies of the Final Structures*

Input to structure calculations			
^{1}H,^{1}H-Distance restraints			
total	29		
intraresidual	8		
sequential	9		
long-range	12		
Dihedral-angle restraints	0		
Results of structure calculations[a])			
Energy [kcal/mol]			
total	103.9	±2.40	99.60 ... 109.41
nonbond	43.2	±1.31	39.47 ... 46.88
restraint	2.9	±0.97	0.81 ... 4.25
NOE violations			
number > 0.1 Å	2.39	±1.05	1 ... 5
number > 0.2 Å	1.16	±0.69	1 ... 3
maximum [Å]	0.24	±0.048	0.073 ... 0.269
sum [Å]	0.62	±0.20	0.277 ... 0.986

[a]) Results are listed as average ± standard deviation and range of observed values (low ... high).

Table 7. *Torsion Angles Found in the* E_{min} *SA Structure* (shown in *Fig. 3*) *and the Predicted and Observed* (given in parentheses) ^{3}J *Values* (see text). Note $\chi_{3'}$ = C(β)–C(γ)–N–C′ torsion in Pro(NH$_2$)[7] and $\chi_{3'}$ = C(β)–C(γ)–C(ε)–C′ in Pro(CH$_2$COOH)[8].

	Torsion angles in the E_{min} SA structure							
	Ala[1]	Asn[2]	Pro[3]	Asn[4]	Ala[5]	Ala[6]	Pro(NH$_2$)[7]	Pro(CH$_2$COOH)[8]
ϕ	–85.0	–100.6	–71.2	–94.7	–59.4	–70.1	–18.8	–18.4
ψ	–66.0	133.8	113.7	169.3	–40.3	–47.1	19.0	18.6
χ_1	–	–71.5	26.4	73.7	–	–	–34.8	–36.8
$\chi_{3'}$							107.3	64.3
	Predicted (observed) coupling constants[a])							
$^3J(\alpha,NH)$	7.3 (4.8)	8.9 (8.1)	–	8.4 (8.4)	4.1 (3.6)	5.5 (5.7)		
$^3J(\alpha,\beta)$	–	12.8 (9.0)	8.5 (7.5)	4.9 (5.2)	–	–	12.0 (8.6)	12.2 (11.5)
		2.4 (5.0)	2.1 (7.1)	3.1 (4.7)			5.7 (7.8)	5.4 (6.0)
$^3J(\beta,\gamma)$	–	–	–	–	–	–	10.7 (6.2)	11.8 (11.5)
							6.3 (6.4)	5.4 (5.8)
$^3J(\gamma,\delta)$	–	–	–	–	–	–	8.6 (7.3)	9.9 (11.8)
							8.5 (4.4)	8.0 (8.3)
$^3J(\gamma,\varepsilon)$								12.3 (9.4)
								2.8 (3.3)

[a]) The $^3J(\alpha,NH)$ and $^3J(\alpha,\beta)$ values were predicted from the observed torsion angles in the minimum energy (E_{min}) SA structure (as given above) and the *Karplus* relationships parameterized for peptides by *Pardi et al.* [17] and *Demarco et al.* [19]. The $^3J(\beta,\gamma)$, and $^3J(\gamma,\varepsilon)$ values were predicted using the *Karplus* equation of *Haasnoot et al.* [14], as implemented in MacroModel v4.5 [18]. The observed coupling constants in parentheses are from *Table 3*.

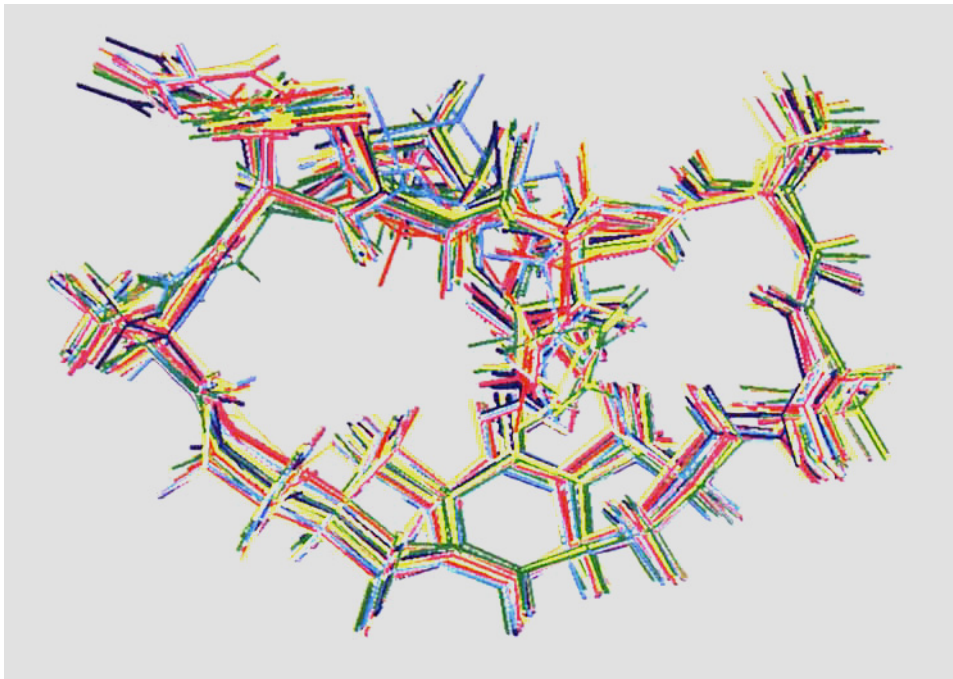

Fig. 2. *Superimposition over the backbone atoms C(α), N, and C′ of the 31 structures for* **6** *derived using restrained simulated annealing* (SA) (see text)

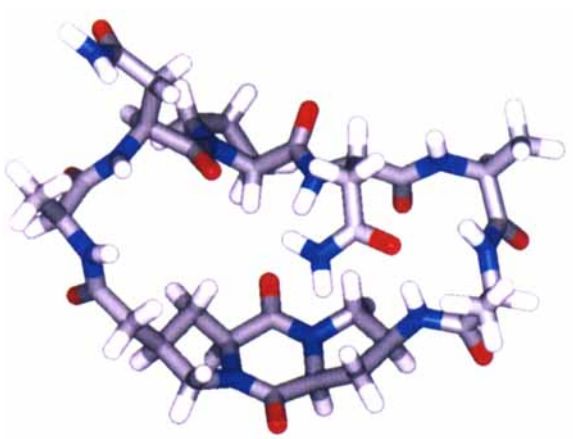

Fig. 3. *The lowest-energy SA structure calculated for* **6**, *viewed as in* Fig. 2 *with the template at the bottom*

backbone CO and its side-chain amide CO group. In addition, H-bonds are formed frequently in these SA structures between the Asn[4] backbone NH and the CO of Pro(CH_2COOH)[8] in the template, as well as between the Ala[6]NH and the Asn[4]CO or Asn[4]O(γ) (see *Fig. 3*). This pattern of intramolecular H-bonding is consistent with the slow H/D exchange of the Asn[4]NH and Pro(NH_2)[7]NH, as well as the low temperature coefficient of the Pro(NH_2)[7] and Ala[6]NH resonances. However, it is then not clear why the Asn[4]NH temperature coefficient is so large (*Table 4*; *vide supra*). On the other hand, a relatively slow H/D exchange rate for an amide proton is clear-cut evidence for shielding from solvent.

Measured and Predicted J *Values*. Since conformational averaging has different influences on NOEs and coupling constants, it is interesting to examine how well the observed ^3J(H,H) values agree with the SA structures deduced for **6**; in a rigid system, NOEs and coupling constants will be consistent with a unique structure, whereas in a dynamic system, NOE restraints will produce a different conformation from that consistent with coupling constants [16]. The observed and predicted [14] [17–19] ^3J(H,H) values for the typical low-energy SA shown in *Fig. 3* are compared in *Table 7*. There is good agreement between the values for $^3J(\alpha,NH)$ apart from Ala[1]. This suggests that the β-turn seen in *Fig. 3* at Asn[4] to Pro(NH_2)[7] is significantly populated, whereas the smaller $^3J(\alpha,NH)$ observed for Ala[1] is consistent with a ϕ-angle for this residue closer to $-65°$. The observed $^3J(\alpha,\beta)$ values for the Asn[2] and Asn[4] residues indicate motion around the C(α)–C(β) bonds, although the coupling constants are not consistent with an equal population of all staggered conformations, for which both $^3J(\alpha,\beta)$ values of *ca.* 6.5–7 Hz would be expected. The $^3J(\alpha,\beta)$ values for Asn[4] indicate that $\chi_1 \approx 60°$ is preferred, which is close to that seen in the SA structure in *Fig. 3*.

This analysis suggests, therefore, that although conformational fluctuations are occurring, the ^3J values observed are generally in reasonable agreement with the structures deduced from NOE data. This strengthens the view that **6** populates stable conformations in aqueous solution that are closely related to the SA structure shown in *Figs. 2* and *3*.

The stable conformations induced by the template in the peptide backbone of **6** are quite different from those found in **3**, where the NPNA motif adopts a stable type-I β-turn [6]. The differences arise from the different geometric properties of the templates in **3** and **6**, but no doubt reflect also the unique H-bonding potential of the hexapeptide sequence ANPNAA. These studies may facilitate the future application of template **5** in the design of novel peptide and protein loop mimetics.

The authors thank the *Swiss National Science Foundation* for financial support.

Experimental Part

General. Flash chromatography (FC): *Merck* silica gel *60* (230–400 mesh). M.p.: uncorrected. $[\alpha]_D$: *Perkin-Elmer-241* polarimeter. IR Spectra: *Perkin-Elmer-781* spectrometer; in cm^{-1}. NMR Spectra: *Bruker-AC300*, *Bruker-ARX300*, or *Bruker-AMX600* for ^1H, and *Varian-XL200* or *Bruker-ARX300* spectrometers for ^{13}C; δ in ppm rel. to $SiMe_4$ as internal standard in $CDCl_3$ or sodium 3-(trimethylsilyl)(D_4)propanoate in H_2O/D_2O, *J* in Hz. MS: chemical ionization (CI) on a *Varian-MAT90* or electrospray ionization (ESI) on a *Finnigan-TSQ700* spectrometer, *m/z* (rel. %).

Peptide Synthesis: *General*. Peptide synthesis was performed on an *LKB-Biolynx-4175* peptide synthesizer. Fmoc-protected amino acids were from *Bachem AG*, Switzerland. Abbreviations: 2-(1*H*-benzotriazol-1-yl)-

1,1,3,3-tetramethyluronium hexafluorophosphate (HBTU), 1-hydroxy-1*H*-benzotriazol (HOBt), 1-hydroxy-1*H*-7-azabenzotriazole (HOAt), 2-(1*H*-azabenzotriazol-1-yl)-1,1,3,3-tetramethyluronium hexafluorophosphate (HATU), 4-methyltrityl (Mtt). Dimethylformamide (DMF) and *N*-methylpyrrolidine (NMP) for peptide synthesis were distilled from ninhydrin prior to use, pyridine was distilled from CaH_2, piperidine from KOH, $(i\text{-}Pr)_2EtN$ from ninhydrin and from KOH. HPLC: dual pump *Pharmacia* system and *Waters-RCM-Bondapak-C_{18}* cartridges (10 mm, 125 Å; 25 × 100 mm) for prep. and (8 × 10 mm) for anal. separations; solvents: *A* H_2O + 0.1% CF_3COOH, and *B*, MeCN + 0.1% CF_3COOH; UV detection at 226 and 254 nm.

(2S,4R)-N-(Benzyloxycarbonyl)-4-hydroxyproline (**8**). To 4-hydroxy-L-proline (30.0 g, 229 mmol) in dioxane (225 ml) and 1M aq. Na_2CO_3 (450 ml) at 0° was added slowly benzyl carbonochloridate (= benzyl chloroformate; 48.7 g, 286 mmol), and the slurry was stirred overnight. Further benzyl carbonochloridate (44.3 g, 140 mmol) was added to ensure complete conversion. The white suspension was then acidified with conc. HCl soln. to pH 2. The soln. was extracted with AcOEt, the org. phase washed with brine and H_2O, dried ($MgSO_4$), and evaporated, and the yellow oil extracted with toluene (100 ml) to remove benzyl alcohol and dried to give **8** (53.6 g, 88%). Colourless crystals. M.p. 104–105°. $[\alpha]_D^{24} = +41.0$ ($c = 1.00$, MeOH). IR (KBr): 3400*s*, 2950*m*, 2070*w*, 1760*s*, 1685*s*, 1500*w*. ^{1}H-NMR (300 MHz, $CDCl_3$): 7.61–7.29 (*m*, 5 H); 5.2 (br. *s*, OH); 5.19–5.11 (*m*, 2 H); 4.57–4.47 (*m*, 2 H); 3.65–3.56 (*m*, 2 H); 2.36–2.09 (*m*, 2 H). CI-MS (NH_3): 283.2 (15, $[M + NH_4]^+$), 266.1 (100, $[M + 1]^+$).

Methyl (2S,4S)-1-[(2S,4R)-1-(Benzyloxycarbonyl)-4-hydroxyprolyl]-4-phthalimidoprolinate. To a soln. of **7** [6] (31.3 g, 80.7 mmol) in CH_2Cl_2 (220 ml), HBTU (31.5 g) was added followed (dropwise) by $(i\text{-}Pr)_2EtN$ (20.5 ml) with stirring at 0°. After 10 min, a soln. of **8** (21.4 g, 80.7 mmol) in CH_2Cl_2 (800 ml) was added. After 4 h, the mixture was washed with 10% aq. citric acid, aq. $NaHCO_3$ soln. and brine. The org. phase was concentrated to a yellow oil and the product crystallized from AcOEt: 28.0 g (65%). M.p. 179–181°. $[\alpha]_D^{24} = -3.3$ ($c = 1.0$, $CHCl_3$). IR (KBr): 3333*m*, 2960*w*, 2890*w*, 1780*m*, 1750*m*, 1740*m*, 1718*s*, 1660*s*. ^{1}H-NMR (300 MHz, $CDCl_3$): 7.84, 7.74 (2*m*, 4 H); 7.43–7.29 (*m*, 5 H); 5.24–3.5 (overlapping signals from 2 conformers, 12 H); 2.47–2.53 (*m*, 2 H); 2.30–2.24 (*m*, 2 H). CI-MS (NH_3): 39.6 (100, $[M + NH_4]^+$), 522.5 (80, $[M + 1]^+$).

(2R,5aS,7S,10aS)-Perhydro-2-hydroxy-7-phthalimido-5H,10H-dipyrrolo[1,2-a:1′,2′-d]pyrazine-5,10-dione (**9**). The foregoing product (28.6 g, 54.8 mmol) and Pd/C (5.6 g) in DMF (380 ml) was stirrd under H_2 (1 atm.) for 6 days. The suspension was filtered through *Celite*, the solvent evaporated, and the residue redissolved in MeOH, which afforded **9** as white crystals (14.0 g, 72%). M.p. 97–98°. $[\alpha]_D^{24} = -37.3$ ($c = 1.0$, DMSO). IR (KBr): 3400*s*, 2970*m*, 2940*m*, 2905*m*, 1770*s*, 1712*s*, 1672*s*, 1640*s*. ^{1}H-NMR: (300 MHz, (D_6)DMSO): 7.87–7.82 (*m*, 4 H); 5.15 (br. *s*, 1 H); 4.94 (*m*, 1 H); 4.60–4.47 (*m*, 2 H); 4.35 (br. *s*, 1 H); 3.83–3.77 (*m*, 1 H); 3.66–3.54 (*m*, 2 H); 3.32–3.25 (*m*, 2 H); 2.69–2.58 (*m*, 1 H); 2.47–2.38 (*m*, 1 H); 2.14–2.00 (*m*, 2 H). ^{13}C-NMR (75 MHz, (D_6)DMSO): 167.45 (*s*); 166.18 (*s*); 165.38 (*s*); 134.34 (*d*); 131.41 (*s*); 122.95 (*d*); 67.31 (*d*); 58.58 (*d*); 58.09 (*d*); 53.55 (*t*); 46.51 (*d*); 45.86 (*t*); 36.46 (*t*); 30.33 (*t*). CI-MS: 356.1 (100, $[M + 1]^+$).

(5aS,7S,10aS)-Perhydro-7-phthalimido-5H,10H-dipyrrolo[1,2-a:1′,2′-d]pyrazine-2,5,10-trione. A soln. of SO_3·pyridine (56 g, 158 mmol; 45% SO_3) in dry DMSO (300 ml) was added to the foregoing product (24.7 g, 69.5 mmol) in dry DMSO (550 ml) and Et_3N (98 ml). After stirring for 6 h, H_2O was added and the pH adjusted to 4.5 using conc. aq. HCl soln. The product was extracted into CH_2Cl_2 and crystallized from CH_2Cl_2: 21.9 g (89%). M.p. 196–198°. $[\alpha]_D^{24} = -54.9$ ($c = 1.0$, DMF). IR (KBr): 3440*w* (br.), 1755*s*, 1715*s*, 1665*s*. ^{1}H-NMR (300 MHz, $CDCl_3$): 7.78 (*m*, 4 H); 5.30–5.00 (*m*, 1 H); 4.73 (*t*, $J = 9.0$, 1 H); 4.46 (*t*, $J = 8.2$, 1 H); 4.32–4.20 (*m*, 2 H); 3.85–3.74 (*m*, 2 H); 3.27–3.17 (*m*, 1 H); 3.06–2.92 (*m*, 2 H); 2.76–2.62 (*m*, 1 H). ^{13}C-NMR (75 MHz, (D_6)DMSO): 208.06 (*s*); 167.95 (*s*); 166.25 (*s*); 165.37 (*s*); 134.82 (*d*); 131.85 (*s*); 123.43 (*d*); 58.29 (*d*); 57.35 (*d*); 52.44 (*t*); 46.62 (*d*); 46.40 (*t*); 39.37 (*t*); 30.71 (*t*). CI-MS: 371.3 (100, $[M + NH_4]^+$), 354.2 (50, $[M + 1]^+$).

Methyl [(5aS,7S,10aS)-Perhydro-5,10-dioxo-7-phthalimido-1H,5H-dipyrrolo[1,2-a:1′,2′-d]pyrazin-2(3H)-ylidene]acetate. To methyl (dimethoxyphosphoryl)acetate (0.9 g, 1.1 equiv.) in dry THF (40 ml) was added 1M sodium bis(trimethylsilyl)amide in THF (6.22 ml, 1.1 equiv.), followed by the foregoing product (1.99 g, 5.62 mmol) in dry DMF (120 ml). After stirring for 5 h at r.t., CH_2Cl_2 (500 ml) was added and the soln. washed with 0.1N aq. HCl and brine. The org. phase was dried (Na_2SO_4) and evaporated: white solid (2.21 g, 96%). M.p. > 220° (dec.). $[\alpha]_D^{24} = +130.0$ ($c = 1.0$, $CHCl_3$). IR ($CHCl_3$): 3010*m*, 1775*m*, 1720*s*, 1680*s*. ^{1}H-NMR (300 MHz, $CDCl_3$): 7.86–7.82, 7.75–7.72 (2*m*, 4 H); 6.97, 6.75 (2*s*, 1 H, C*H*COOMe (*cis*/*trans*)); 5.04 (*quint.*, 1 H); 4.76–4.70, 4.45–4.39 (2*m*, 2 H); 4.13–4.06, 3.86–3.81 (2*m*, 2 H); 3.73 (*s*, MeO); 3.29–3.01 (*m*, 5 H); 2.60–2.58 (*m*, 1 H). CI-MS: 410.0 (100, $[M + 1]^+$).

Methyl [(2R,5aS,7S,10aS)-Perhydro-5,10-dioxo-7-phthalimido-1H,5H-dipyrrolo[1,2-a:1′,2′-d]pyrazin-2-yl]acetate. The foregoing product (2.21 g, 5.18 mmol) in MeOH (90 ml) and AcOEt (60 ml) with 10% Pd/C (0.2 g) was stirred under H_2 (1 atm) for 48 h. After filtration through *Celite* and evaporation, the resulting green oil was subjected to FC (AcOEt): oil (1.40 g, 60%). $[\alpha]_D^{24} = -28.0$ ($c = 1.0$, $CHCl_3$). IR ($CHCl_3$): 3005*m*, 2960*m*, 1780*m*, 1715*s*, 1670*w*, 1615*w*. ^{1}H-NMR (300 MHz, $CDCl_3$): 7.86–7.72 (*m*, 4 H); 5.01 (*m*, 1 H); 4.42–4.30 (*m*, 2 H);

4.15–4.09 (*m*, 1 H); 3.88–3.68 (*m*, 5 H); 3.32–3.25 (*m*, 1 H); 3.04–2.92 (*m*, 1 H); 2.78–2.72 (*m*, 1 H); 2.64–2.51 (*m*, 4 H); 2.02–1.90 (*m*, 1 H). ^{13}C-NMR (75 MHz, $CDCl_3$): 169.94 (*s*); 165.48 (*s*); 163.73 (*s*); 163.11 (*s*); 132.16; 129.48; 121.37; 58.12 (*d*); 57.22 (*d*); 49.69 (*d*); 48.24 (*t*); 44.97 (*t*); 44.86 (*d*); 35.18 (*t*); 31.93 (*t*); 31.07 (*q*); 29.18 (*t*). Cl-MS: 429 (44, $[M + NH_4]^+$), 412 (100, $[M + 1]^+$).

*(2*R*,5a*S*,7*S*,10a*S*)-7-{[(9*H*-Fluoren-9-ylmethoxy)carbonyl]amino}perhydro-5,10-dioxo-1*H*,5*H*-dipyrrolo-[1,2-a:1′,2′-d]pyrazine-2-acetic Acid* (**5**). The foregoing product (500 mg, 1.22 mmol) in MeOH (7.5 ml) and hydrazine hydrate (60.8 mg, 1.22 mmol) was stirred overnight at r.t. After filtration and evaporation, the residue was dissolved in EtOH (12 ml), and a soln. of LiOH (130 mg, 3 equiv.) in H_2O (6 ml) was added. After 48 h, the pH was adjusted to 7 (dil. HCl soln.), the soln. evaporated, and the residue redissolved in dioxane (20 ml) and 1M aq. Na_2CO_3 (24 ml). At 0°, 9*H*-fluoren-2-ylmethyl carbonochloridate (620 mg, 2 equiv.) in dioxane (20 ml) was added at 0°, and the slurry was stirred for 18 h. The mixture was acidified (pH 1) and extracted with AcOEt, the org. phase evaporated and the residue crystallized from MeOH: **5** (328 mg, 55%). M.p. > 230° (dec.). ^{1}H-NMR (600 MHz, (D_6)DMSO): 12.03 (br. *s*, 1 H); 7.89–7.30 (*m*, 8 H); 7.55 (*d*, 1 H); 4.35–4.31 (*m*, 4 H); 4.23–4.15 (*m*, 2 H); 3.80 (*m*, 2 H); 3.13–3.08 (*m*, 1 H); 3.03–2.98 (*m*, 1 H); 2.53–2.48 (*m*, 1 H); 2.38 (*d*, 2 H); 2.35–2.22 (*m*, 2 H); 1.95–1.87 (*m*, 1 H); 1.70–1.61 (*m*, 1 H). ESI-MS: 512.5 (100, $[M + Na]^+$), 490.3 (50, $[M + 1]^+$).

Cyclo(-Ala-Asn-Pro-Asn-Ala-Ala Pro(NH$_2$) = Pro(CH$_2$COOH)) (**6**). Fmoc-Ala-OH coupled to 4-alkoxy-2-methoxybenzyl alcohol (*TentaGel-S AC*) resin (*Rapp Polymere GmbH*, Tübingen; 1.0 g, 0.24 mmol/g) was used to initiate synthesis, with coupling first of Pro(NHFmoc) = Pro(CH_2COOH) (**5**) (*Scheme 4*). Fmoc-Ala-OH, Fmoc-Asn(Mtt)-OH, and Fmoc-Pro-OH (each 1 mmol) were used for chain elongation and HOBt/HBTU for activation [20]. The completion of each coupling cycle was monitored by ninhydrin [21] or isatin [22] tests. If these tests revealed incomplete coupling, the coupling reaction was repeated; the coupling of Fmoc-Ala-OH onto the template was performed twice, and the last coupling of Fmoc-Asn(Mtt)-OH three times. Upon completion of the synthesis, the N-terminal Fmoc-protecting group was removed with 20% piperidine in DMF, the resin was washed with MeOH, dried, and reswollen in CH_2Cl_2 for 10 min. The peptide was cleaved from the resin with 1% CF_3COOH/CH_2Cl_2. After 20 min, the soln. was filtered and neutralized in pyridine/MeOH. After evaporation, HPLC (30–95% solvent B over 30 min) gave the side-chain-protected product H-Asn(Mtt)-Pro-Asn(Mtt)-Ala-Ala Pro(NH_2) = Pro(CH_2COOH) Ala-OH (**10**; 112 mg, 38%). ESI-MS: 1319 (100, $[M + H]^+$). This product (112 mg, 0.086 mmol) in DMF (70 ml) was treated with HATU (182 mg, 0.482 mmol), HOAt (672 mg, 0.482 mmol), and (i-Pr)$_2$EtN (2.46 ml) in 70 ml DMF. After 24 h at r.t., the soln. was evaporated, the residue taken up in MeCN, and the product purified by HPLC (30–95% solvent *B* over 30 min): 89 mg (80%). ESI-MS: 1301 (25, $[M + H]^+$). This product (80 mg) was stirred in $CF_3COOH/H_2O/Me_3SiH$ 95:2.5:2.5 at r.t. for 6 h. The soln. was evaporated and the residue taken up in H_2O and washed with (i-Pr)$_2$O. Product **6** was purified by HPLC (0–40% *B* over 20 min): 24.1 mg (50%). ESI-MS: 788 (25, $[M + H]^+$).

NMR and SA Calculations. Structure calculations were performed by the method described previously [6]. Cross-peak volumes were quantitated in ROE spectra (ROESY) with 75, 150, 225, 300, and 375 ms mixing times using the FELIX software (*Biosym*, San Diego). The ROESY cross-peak intensities were corrected for resonance offset effects, as described by *Griesinger* and *Ernst* [23] for medium-size molecules. Distances were calibrated using $H_{pro\text{-}S}$–$H_{pro\text{-}R}$ at C(δ) in Pro(CH_2COOH)[8] of 1.78 Å and calculating other distances according to the r^{-6} relationship, using three models: *1*) assuming a linear NOE buildup to 225 ms mixing time and using the cross-peak volumes at 225 ms to determine distances; *2*) fitting a straight line to the buildup curve, from which distances were then extracted; *3*) fitting the buildup curve to a second-order polynomial function. The agreement between these methods was good. Distances determined as $\leq$ 2.5 Å were set to 2.7 Å, those > 2.5 Å but < 3.0 Å were set to 3.2 Å, and those > 3.0 Å were set to 5.0 Å. The necessary pseudoatom corrections were applied for Me groups, and the resulting values were used as input upper distance restraints. NOE restraint violations were penalized with a weighting factor of 15 kcal/mol/Å^2 with an upper limit of 250 kcal/mol/Å.

The calculations were initiated with an arbitrary starting conformation. Fifty calculations were performed differing in the values of the random number seed, to generate different initial velocities for all atoms. Each calculation then consisted of initial energy minimization (100 steps steepest descent), 45 ps of molecular dynamics at 1000 K, during which first the NOE force constants and then the internal force constants were scaled up, 15 ps of molecular dynamics during cooling to 300 K, energy minimization (100 steps steepest descent, 100 steps conjugate gradient, 100 steps quasi-*Newton-Raphson*), 5 ps of molecular dynamics at 300 K, and a final energy minimization (100 steps steepest descent, 100 steps conjugate gradient, 1000 steps quasi-*Newton-Raphson*). The *van der Waals* potential was set to a quartic form during the SA procedure and changed to the normal *Lennard-Jones* potential for energy minimization. A cut-off distance of 10 Å for nonbonded interactions was used. Charges and cross terms were not included during dynamics, but in the final stages of minimization, both were included, using a distance-dependent dielectric scaled by a factor of 4 × *r*. Constraints were applied to avoid inversions at chiral centres and the conversion of *trans* to *cis* peptide bonds or *vice versa*.

X-Ray Structure Analysis of **5**[2]). $C_{27}H_{27}N_3O_6 \cdot MeOH$. All measurements were conducted at low-temperature on a *Rigaku-AFC5R* diffractometer using graphite-monochromated CuK_α radiation ($\lambda = 1.54178$ Å) and a 12 kW rotating anode generator. The intensities were collected using $\omega/2\theta$ scans. Three standard reflections which were measured after every 150 reflections remained stable throughout the data collection. The intensities were corrected for *Lorentz* and polarization effects, and a semi-empirical absorption correction [24] was applied. The structure was solved by direct methods using SHELXS86 [25] which revealed the position of all non-H-atoms of two symmetry-independent molecules of **5** and two molecules of MeOH. The non-H-atoms were refined anisotropically. All of the H-atoms bonded to C-atoms were fixed in geometrically calculated positions with a C–H distance of 0.95 Å. The H-atoms bonded to N-atoms and O-atoms were fixed in the positions indicated by a difference electron density map. Each H-atom was assigned a fixed isotropic temperature factor with a value of 1.2 U_{eq} of the atom to which it was bonded. H-Atoms were not included for the solvent molecules. All refinements were carried out on F using full-matrix least-squares procedures which minimized the function $\Sigma w(|F_o| - |F_c|)^2$, where $w = [\sigma^2(F_o) + (0.005F_o)^2]^{-1}$. The data collection and refinement parameters are given in *Table 8*. All calculations were performed using the TEXSAN [26] crystallographic software package, and *Fig. 1* was produced with ORTEPII [27].

Table 8. *Crytallographic Data for* **5**

Crystallized from	MeOH
Empirical formula	$C_{27}H_{27}N_3O_6 \cdot CH_3OH$
Formula weight	521.57
Crystal colour, habit	colourless, plate
Crystal dimensions [mm]	0.08·0.28·0.50
Temperature [K]	298 (1)
Crystal system	orthorhombic
Space group	$P2_12_12_1$
Lattice parameters	
Reflections for cell determination	25
2θ range [°]	81–93
a [Å]	17.614 (1)
b [Å]	40.777 (3)
c [Å]	7.232 (2)
V [Å^3]	5194 (1)
Z	8
D_x [g cm^{-3}]	1.334
Absorption coefficient μ (CuK_α) [mm^{-1}]	0.800
Transmission factors (min; max)	0.905; 1.000
$2\theta_{(max)}$ [°]	120
Total reflections measured	5339
Symmetry-independent reflections	5173
R_{int}	0.020
Reflections observed ($I > 2\sigma(I)$)	4136
Variables	685
Final R	0.1061
R_w	0.1025
Weights	$[\sigma^2(F_o) + (0.005F_o)^2]^{-1}$
Goodness of fit	4.748
Final δ_{max}/σ	0.04
$\Delta\rho$ (max; min) [2 Å^{-3}]	0.38; −0.36

[2]) Crystallographic data (excluding structure factors) for the structures reported in this paper have been deposited with the *Cambridge Crystallographic Data Centre* as supplementary publication No. CCDC-10/27. Copies of the data can be obtained, free of charge, on application to the Director, CCDC, 12 Union Road, Cambridge CB2 1EZ, UK (fax: +44 (0) 1223 336033, or e-mail: teched@chemcrys.cam.ac.uk).

The solvent molecules are probably disordered or undergoing strong motion within their cavity, as seen from their enlarged thermal parameters, and it may be that the C- and O-atoms have been incorrectly assigned; however, further resolution of the solvent disorder was not possible. The high R factors and the poor accuracy of the refinement results are attributed to crystal quality. Repeated determinations from three different crystals produced results of similar quality, and a better sample could not be obtained.

REFERENCES

[1] M. Mutter, G.G. Tuchscherer, C. Miller, K.-H. Altmann, R.I. Carey, D.F. Wyss, A.M. Labhardt, J.E. Rivier, *J. Am. Chem. Soc.* **1992,** *114,* 1463.

[2] G.L. Olson, B.D.R., M.P. Bonner, M. Bös, C.M. Cook, D.C. Fry, B.J. Graves, M. Hatada, D.E. Hill, M. Kahn, V.S. Madison, V.K. Rusiecki, R. Sarabu, J. Sepinwall, G.P. Vincent, M.E. Voss, *J. Med. Chem.* **1993,** *36,* 3039.

[3] K. Müller, D. Obrecht, A. Knierzinger, C. Stankovic, C. Spiegler, W. Bannwarth, A. Trzeciak, G. Englert, A.M. Labhardt, P. Schönholzer, in 'Perspectives in Medicinal Chemistry', Eds. B. Testa, E. Kyburz, W. Fuhrer, and R. Giger, Verlag Helvetica Chimica Acta, Basel, 1993, p. 513-531.

[4] S. Jackson, W. DeGrado, A. Dwivedi, A. Parthasarathy, A. Higley, J. Krywko, A. Rockwell, J. Markwalder, G. Wells, R. Wexler, S. Mousa, R. Harlow, *J. Am. Chem. Soc.* **1994,** *116,* 3220.

[5] F. Emery, C. Bisang, M. Favre, L. Jiang, J.A. Robinson, *J. Chem. Soc., Chem. Commun.* **1996,** 2155.

[6] C. Bisang, C. Weber, J.A. Robinson, *Helv. Chim. Acta* **1996,** *79,* 1825.

[7] H.J. Dyson, A.C. Satterthwait, R.A. Lerner, P.E. Wright, *Biochemistry* **1990,** *29,* 7828.

[8] C. Bisang, C. Weber, J. Inglis, C.A. Schiffer, W.F. van Gunsteren, I. Jelesarov, H.R. Bosshard, J.A. Robinson, *J. Am. Chem. Soc.* **1995,** *117,* 7904.

[9] O. Mitsunobu, M. Wada, T. Sano, *J. Am. Chem. Soc.* **1972,** *94,* 679.

[10] E. Atherton, R.C. Sheppard, 'Solid Phase Peptide Synthesis – a Practical Approach', IRL Press, Oxford, 1989.

[11] L.A. Carpino, *J. Am. Chem. Soc.* **1993,** *115,* 4397.

[12] K. Wüthrich, 'NMR of Proteins and Nucleic Acids', J. Wiley & Sons, New York, 1986.

[13] G. Merutka, H.J. Dyson, P.E. Wright, *J. Biol. NMR* **1995,** *5,* 14.

[14] C.A.G. Haasnoot, F.A.A.M. De Leeuw, C. Altona, *Tetrahedron* **1980,** *36,* 2783.

[15] M. Nilges, A.M. Gronenborn, A.T. Brünger, G.M. Clore, *Protein. Eng.* **1988,** *2,* 27.

[16] M. Eberstadt, G. Gemmecker, D.F. Mierke, H. Kessler, *Angew. Chem. Int. Ed.* **1995,** *34,* 1671.

[17] A. Pardi, M. Billeter, K. Wüthrich, *J. Mol. Biol.* **1984,** *180,* 741.

[18] F. Mohamadi, N.G.J. Richards, W.C. Guida, R. Liskamp, M. Lipton, C. Caufield, G. Chang, T. Hendrickson, W.C. Still, *J. Comput. Chem.* **1990,** *11,* 440.

[19] A. Demarco, M. Llinás, K. Wüthrich, *Biopolymers* **1978,** *17,* 617.

[20] R. Knorr, A. Trzeciak, W. Bannwarth, D. Gillessen, *Tetrahedron Lett.* **1989,** *30,* 1927.

[21] V.K. Sarin, S.B.H. Kent, J.P. Tam, R.B. Merrifield, *Anal. Biochem.* **1981,** *117,* 147.

[22] E. Kaiser, C.D. Bossinger, R.L. Colescott, D.B. Olsen, *Anal. Chim. Acta* **1980,** *118,* 149.

[23] C. Griesinger, R.R. Ernst, *J. Magn. Reson.* **1987,** *75,* 261.

[24] A.C.T. North, D.C. Phillips, F.S. Mathews, *Acta Crystallogr., Sect. A* **1968,** *24,* 351.

[25] G.M. Sheldrick, 'SHELXS86', *Acta Crystallogr., Sect. A* **1990,** *46,* 467.

[26] 'TEXSAN, Single Crystal Structure Analysis Software, Version 5.0', Molecular Structure Corporation, The Woodlands, Texas, 1989.

[27] C.K. Johnson, 'ORTEPII. Report ORNL-5138', Oak Ridge National Laboratory, Oak Ridge, Tennessee, 1976.